## Electronic Supplementary Materials

For https://doi.org/10.1631/jzus.A2300398

# Design and experimental validation of an electromagnetic launching mechanism for a tethered net

Zongming ZHU, Weihao LUO, Zongjing LIN, Yuzhe KANG, Maoying ZHOU✉, Ban WANG✉, Huawei QIN

*School of Mechanical Engineering, Hangzhou Dianzi University, Hangzhou 310018, China*

✉ Maoying ZHOU, myzhou@hdu.edu.cn

Ban WANG, bigban@zju.edu.cn

### S1 Theoretical model of the reluctance coil launching unit

In this process, if we neglect the air resistance and friction experienced by the projectile, the conservation of energy is expressed as:

$$\frac{1}{2}CU_p^2=\frac{1}{2}Cu^2(t)+\int_0^t i(\tau)^2\,d\tau+W_m+\frac{1}{2}mv_e^2+W_{fric} \quad (S1)$$

where $U_p$ and $C$ are the initial charged voltage and capacitance of the capacitor respectively, $u(t)$ is the voltage across the capacitor at time $t$, $i(\tau)$ is the instantaneous current flowing through the coil at time instant $\tau$, $R$ is the total electrical resistance of the coil, $\int_0^t i(\tau)^2\,R d\tau$ denotes the joule heat loss up to the time instant $t$, $W_{fric}$ is the work done by frictional forces in the process of launching, $W_m$ is the magnetic energy stored in the whole system, and $\frac{1}{2}mv_e^2$ represents the kinetic energy of projectile at the exit of the launching tube with $m$ and $v_e$ being the mass and exit velocity of the projectile.

In the actual operation of the coil launcher, a comprehensive discussion of the launching properties should involve a detailed check of the magnetic field in the system and the electrical discharging circuit consisting of the capacitor and the coil. However, for an approximate description of the launching process, it can be assumed that the remanent voltage upon the capacitor is much smaller than $U_p$. In this sense, $\frac{1}{2}Cu^2(t)$ can be omitted in the approximate calculation. Further, at the end of the launching process, the current in the coil is much smaller than its initial value. Since magnetic energy stored in the system is closely related to the current in the coil, $W_m$ can also be neglected and so does the joule heat $\int_0^t i(\tau)^2\,R d\tau$. In this sense, we approximately express the exit velocity $v_e$ as:

$$v_e=\sqrt{\frac{C}{m}U_p^2-\frac{2W_{fric}}{m}} \quad (S2)$$

## S2 Motion of the projectile and the tethered net

According to the Morris equation(Beji, 2019), the drag of a cylindrical projectile in the air is:

$$F_{drag}=C_d S\frac{\rho_{air}v^2}{2}+\rho_{air}\frac{\pi D_p^2}{4}C_m\frac{dv}{dt} \quad (S3)$$

where $C_d$ is the aerodynamic drag coefficient and taken as 0.8(Blevins, 1977), $C_m$ is the coefficient of the inertial and taken as 1.8(Blevins, 1977). $S$ is the bottom area of the projectile. $\rho_{air}$ is the density of air and taken as $1.29\ kg/m^3$, $D_p$ is the diameter of the projectile.

Things become complex when we consider the tension $F_{tension}$ applied to the projectiles by the tethered net. It is actually determined by the interaction between the projectiles and the tethered net in the flight. However, the geometric shape, spatial topology, and unfolding state of the tethered net is time varying and hard to deal with in the presence of some theoretical difficulties. To name a few, overall rheology of the tethered net is largely affected by the materials and mesh structures of the tethered net and differs significantly between the partially folded state and fully unfolded state.

The projectile flies in the air under the action of gravity, air drag $F_{drag}$ and tension $F_{tension}$ from the connecting thread, as shown in Fig. S1. Remembering that the tethered net is used for capturing objects, some simplifications can then be made. Firstly, unfolding process of the tethered net is exclusively considered when talking about the dynamics of the tethered net. This is actually reasonable. In the practical operation of the launching system, we can always adjust the distance between the launching system and the object so that the launched tethered net contacts the object before fully unfolded. Secondly, in the unfolding process of the tethered net, the reactive tension $F_{tension}$ is much smaller compared with the gravity and aerodynamic drag. This is true if we noticed that the partially unfolded tethered net can only provide very limited elastic tension and the mass of the tethered net is much smaller than that of the projectiles. In this sense, we can actually neglect $F_{tension}$ without introducing significant errors.

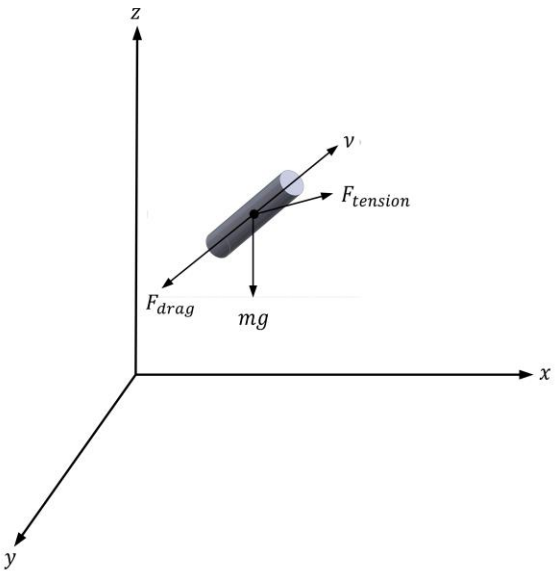


**Fig. S1 The projectile in the flight under the action of different forces.**

Neglecting the reactive tension $F_{tension}$, the motion of one projectile can be sketched in a two-dimensional way. Indeed, as the gravity force is always in the vertical direction towards the earth, and the air drag $F_{drag}$ is always in the opposite direction of the current velocity vector, the y axis can be chosen as the opposite direction of gravity, and the x axis can be chosen as perpendicular to the y axis and pointing towards the moving direction of the projectile. The origin

of the coordinate system is chosen at the exit of the tube. In this way, the position of the projectile is represented by the coordinates $(x, y)$ with a parameter to denote the angle between the velocity vector and the positive $x$ axis defined by $\tan\theta = dy/dx$. The governing equation of the motion of the projectile is then:

$$\begin{cases} \dot{x}\cos\theta = v_x \\ \dot{x}\sin\theta = v_y \\ m\dfrac{dv_x}{dt} = \left(C_d S\dfrac{\rho_{air}v^2}{2} + \rho_{air}\dfrac{\pi D_p^2}{4}C_m\dfrac{dv}{dt}\right)\cos\theta \\ m\dfrac{dv_y}{dt} = \left(C_d S\dfrac{\rho_{air}v^2}{2} + \rho_{air}\dfrac{\pi D_p^2}{4}C_m\dfrac{dv}{dt}\right)\sin\theta - mg \end{cases} \qquad (S4)$$

where $v_x = \dot{x}\cos\theta$ and $v_y = \dot{x}\sin\theta$ are the x-component and y-component of the velocity vector, and $g$ is the local gravitational acceleration with $g = 9.81\ m/s^2$ adopted.

## S3 Experimental setup of projectile exit velocity

The geometrical structure of the designed reluctance coil launching unit is shown in Fig. S2(a). The main body of the launching tube is 3D printed using ABS resin. The coil is prepared using a winding machine upon the tube to guarantee the uniformity and consistency of the properties of different launching units. The projectiles are made from commercially available cylinder pins, whose mass is around 8 g with a diameter of 8 $mm$ and a length of 25 $mm$.

The measuring system consists of a launching tube, the projectile, and a tachymeter, as shown in Fig. S2(b). The exit velocity of the projectile is measured using a tachymeter(HT-X3006), which is mounted to the exit of the launching tube. Initially, the projectile is placed in such a way that the head of the projectile coincides with the tail of the coil, as shown in. The tachymeter uses an optical principle to measure the velocity of the projectile. It mainly consists of two photoelectric switches (switch 1 and switch 2) that are normally open and some distance apart. While the projectile moves through switch 1 or switch 2, the corresponding switch is turned off and a switching signal is detected. The time difference between the two detected switching signals can then be obtained. And the exit velocity of the projectile is calculated using the distance between the two switches and the time difference between the two switching signals.

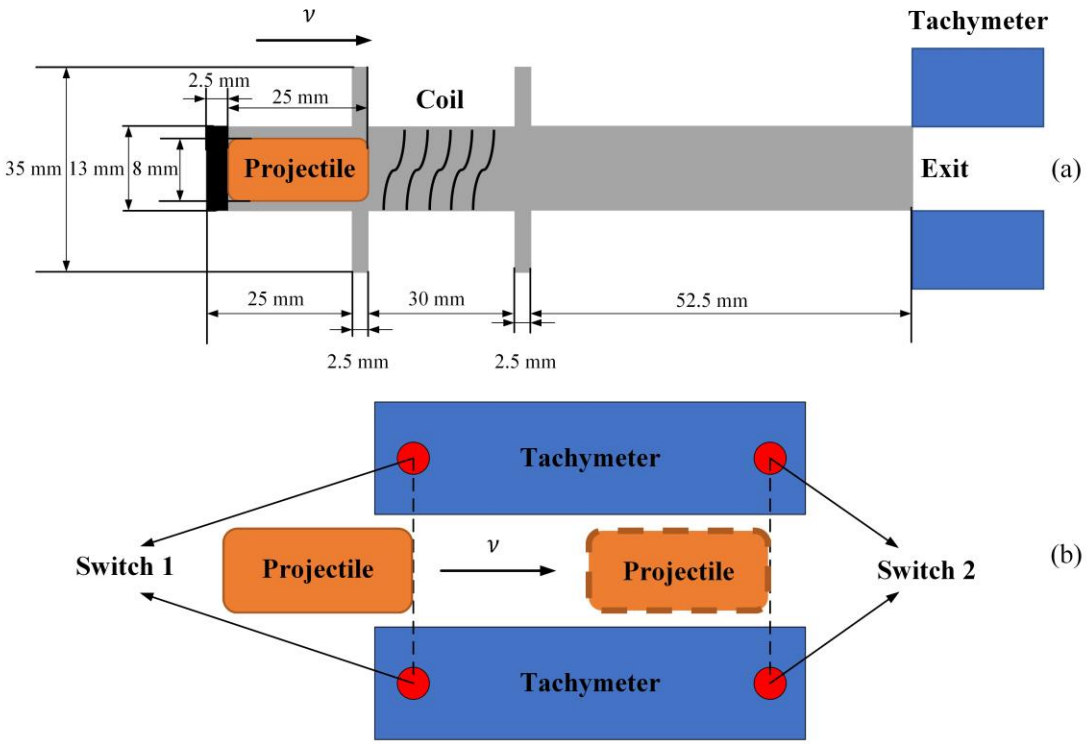


**Fig. S2 Schematic diagram of the exit velocity measurement experiment. (a) geometric description of the reluctance coil launching unit, (b) principle of velocity measurement.**

## S4 The calculation process of theoretical current

With changing charged voltage, the currents during the launching process are plotted in a single figure versus time. As shown in Eq. (S1), if we omit the velocity of the projectile, and express the energy stored in the coil as:

$$W_m=\frac{1}{2}L_c\, i^2(t) \quad (S5)$$

The circuit of reluctance coil launcher can be simplified to RCL circuit and can be expressed as:

$$u(t)=R_c\cdot i(t)+L_c\frac{di(t)}{dt} \quad (S6)$$

Then the governing equations of the current in the coil can be obtained by differentiating the two sides of Eq.(S6) with respect to time t as:

$$\frac{d^2u(t)}{dt^2}=\frac{-u(t)-C\cdot R_c\frac{du(t)}{dt}}{C\cdot L_c} \quad (S7)$$

## S5 Flight of the projectiles and the tethered net

The experiment setup for the flight of the projectiles and the tethered net is shown in Fig. S3. Two coordinate boards are set perpendicular to each other and help record the spatial coordinates of the projectiles. One coordinate board is placed horizontally to record the projected positions of the projectiles in the x-y coordinate plane, and the other coordinate board is placed vertically to record their projected positions in the x-z coordinate plane. Each grid in both coordinate boards is a square with the side length of 1.25 cm. The coordinate range of the established coordinate system is 0-200 cm in the x direction, 0-80 cm in the y direction, and 0-200 cm in the z direction.

The friction coefficient between the projectile and the inner wall of the launching unit was 0.5. Before the experiment began, the launching prototype is placed on the built experimental platform, where the center of the storage is (15,35,22.5) in the defined coordinate system. Meanwhile, two mobile phones of the same brand(Huawei Mate30) are adopted in the experimental setup to capture motion videos of the projectiles. One mobile phone is placed vertically 200 cm away from the horizontal coordinate board while the other one is placed vertically 140 cm away from the vertical coordinate board. Two spirit levels are attached to the mobile phones respectively to guarantee their orientations. In the experiment, the same 60 fps frame rate and 1080p resolution are used in the video on both mobile phones. Before the projectiles are about to be launched, the two mobile phones are triggered simultaneously to record the motion videos by a remote control device(UGREEN LP354).

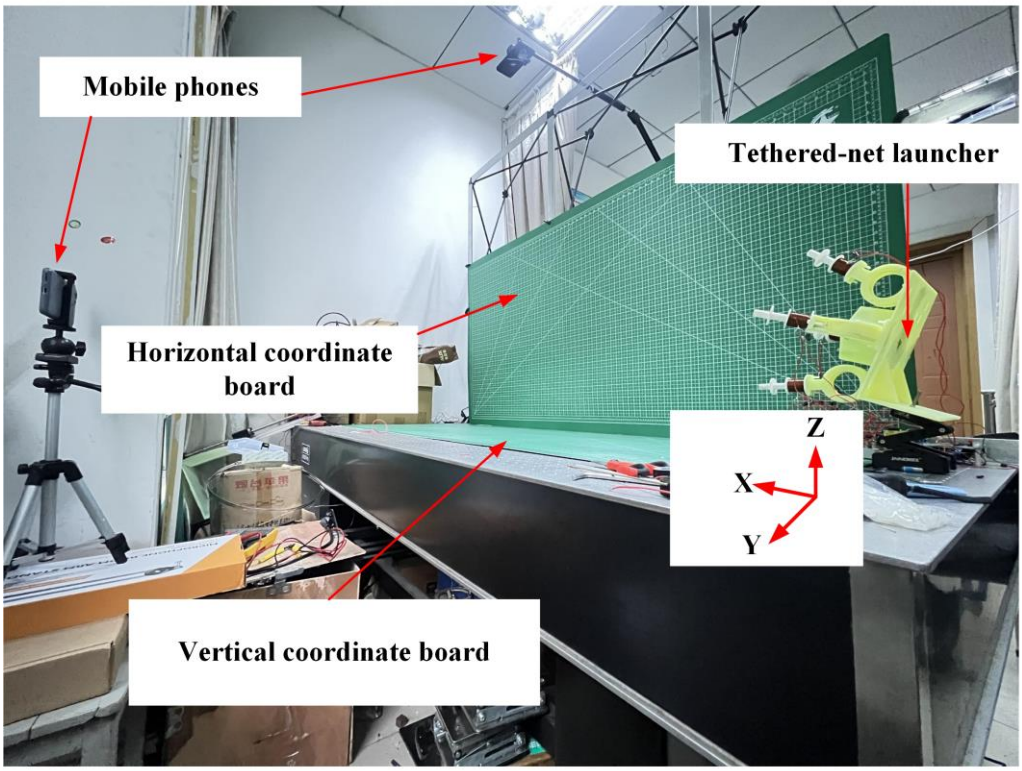


**Fig. S3 Experiment setup for the flight of the projectiles and the tethered net.**

The observation experiment of the trajectory of the projectiles is carried out respectively for the above four connection modes. Before launching the projectiles, the Bluetooth remote control module is used to control two mobile phones to start recording at the same time. Then the projectiles are launched through the discharging switch, and the video recording is finished after the projectiles land. After the recording, the video will be clipped and slowed down and the duration of each video will be limited to 5 s. Since the video frames is 60 frames, the total number of frames of each video is 300 frames. Then the OpenCV library is used for video frame processing. In order to observe the coordinate information more accurately, the time interval between each picture is set to 10 ms. So 30 pictures of the projectiles at different moments are obtained. The coordinates of the projectiles in the x-z coordinate plane can be obtained by the horizontal mobile phone, and the coordinates of the projectile in the x-y coordinate plane can be obtained by the vertical mobile phone. Finally, the three-dimensional coordinate information of the projectiles at different time can be obtained by combining the coordinate of horizontal and vertical position. In order to eliminate the systematic error of the experiment, the coordinates of the projectiles were measured five times in each group of experiments and then the average value was taken.

## S6 Experimental analysis of the three connection patterns

The first experiment is conducted for the double-projectile connection pattern. The adopted projectiles are launched by the coil 1 and coil 3 and painted red and yellow, respectively. With the charged voltage of the capacitor to be 100 V, three different launching angles ($\alpha=0^\circ$, $\alpha=10^\circ$, $\alpha=20^\circ$ ) are adopted. The obtained three-dimensional coordinates of the two projectiles are plotted together, as shown in Fig. S4. It is seen from the figure that when the launching angle $\alpha=0^\circ$, projectile No. 1 lands at time instant of 120 ms, while projectile No. 3 lands at time instant of 110 ms. When the launching angle $\alpha=10^\circ$, projectile No. 1 bounces back at time instant of 130 ms and lands at 140 ms, while projectile No. 3 bounces back at 130 ms and lands at 160 ms. When the launching angle $\alpha=20^\circ$, projectile No. 1 bounces back at 150 ms and lands at 170 ms, while projectile No. 3 bounces back at 160 ms and lands at 170 ms. It should be noted that the coordinates of the projectiles after landing are not analyzed and marked as 0 instead. From the experimental results, when the launching angle $\alpha=0^\circ$, both projectiles move in the positive direction of the x axis. So the tension of the fishing line will not affect the motion of the projectiles and there will be no rebound phenomenon. When the launching angle $\alpha=10^\circ$ and $\alpha=20^\circ$, the two projectiles are subjected to the tension of the fishing line and produce a rebound phenomenon after reaching the maximum opening length of the fishing line.

Next, the projectiles in the square pattern are investigated. The recorded coordinates of the projectiles in flight are plotted in Fig. S5 at different launching angles. When the launching angle $\alpha=0^\circ$, the four projectiles No. 1, No. 2, No. 3, and No.4 land at 150 ms, 100 ms, 150 ms, and 180 ms, respectively. When the launching angle $\alpha=10^\circ$, projectile No. 1 bounces back at 100 ms and lands at 190 ms, projectile No. 2 lands at 120 ms, projectile No. 3 bounces back at 130 ms and lands at 160 ms, and projectile No. 4 bounces back at 110 ms and lands at 240 ms. When the launching angle $\alpha=20^\circ$, projectile No. 1 bounces back at 90 ms and lands at 240 ms, projectile No. 2 lands at 200 ms, projectile No. 3 bounces back at 110 ms and lands at 250 ms, and projectile No. 4 bounces back at 100 ms and lands at 230 ms. It can be seen from the experimental results that when the launching angle $\alpha=0^\circ$, the four projectiles all move in the positive direction of the x axis and there will be no rebound phenomenon. when the launching angles $\alpha=10^\circ$ and $\alpha=20^\circ$, due to the tension of the fishing line between the four projectiles, projectiles No. 1, No. 3, and No. 4 bounce back after the four fishing lines reach the maximum opening area.

As for the case of the cross pattern, apart from the square pattern, the red and yellow projectiles are connected, and the blue and purple projectiles are connected. Flight coordinates of the projectiles are plotted together, as shown in Fig. S6. When the launching angle $\alpha=0^\circ$, projectile No. 1 lands at 140 ms, projectile No. 2 lands at 120 ms, projectile No. 3 lands at 140 ms, and projectile No. 4 lands at 190 ms; When the launching angle $\alpha=10^\circ$, projectile No. 1 bounces back at 130 ms and lands at 160 ms, projectile No. 2 lands at 120 ms, projectile No. 3 bounces back at 170 ms and lands at 200 ms, and projectile No. 4 bounces back at 110 ms and lands at 200 ms. When the launching angle $\alpha=20^\circ$, projectile No. 1 bounces back at 110 ms and lands at 220 ms, projectile No. 2 lands at 170 ms, projectile No. 3 bounces back at 120 ms and lands at 230 ms, and projectile No. 4 bounces back at 100 ms and lands at 230 ms. It can be seen that when the launching angle $\alpha=0^\circ$, the four projectiles all move in the positive direction of the x axis and the tension of the fishing line will not affect the motion of the projectiles. When the launching angles $\alpha=10^\circ$ and $\alpha=20^\circ$, projectiles No. 1, No. 3, and No. 4 bounce back rapidly after the four projectiles are maximally separated. Different from the square pattern, four projectiles bounce back faster in the cross pattern. This is mainly due to the tension of the diagonal fishing lines , causing the two projectiles on the diagonal to bounce faster.

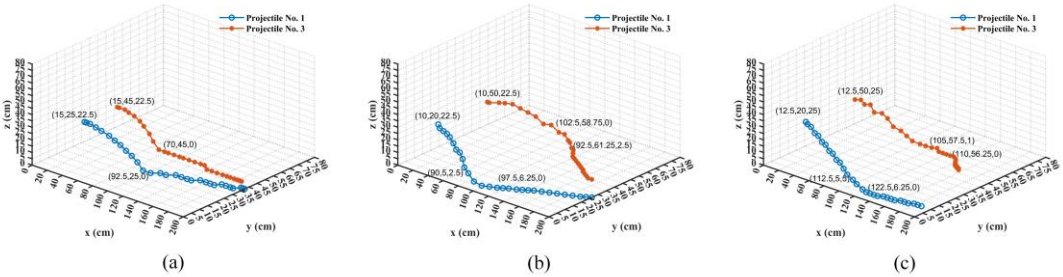


**Fig. S4 Flight trajectories of the projectiles in the double-projectile pattern (The initial, bounce-back and landing coordinates of the projectile are marked in the figure.). (a) α=0˚, (b) α=10˚, (c) α=20˚**

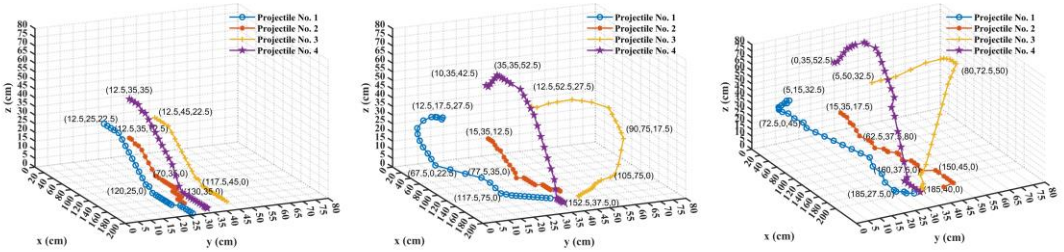


**Fig. S5 Flight trajectories of the projectiles in the square pattern (The initial, bounce-back and landing coordinates of the projectile are marked in the figure.). (a) α=0˚, (b) α=10˚, (c) α=20˚**

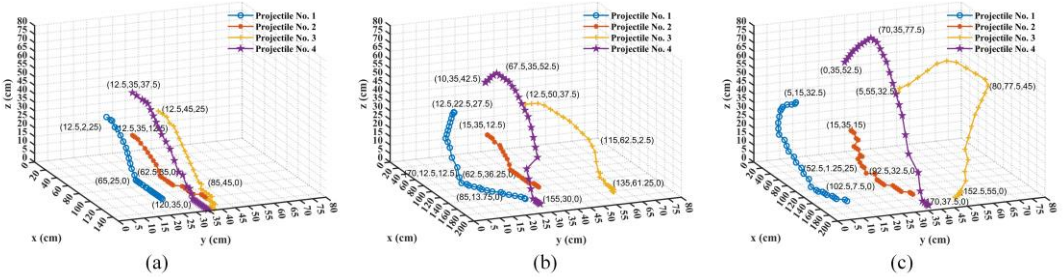


**Fig. S6 Flight trajectories of the projectiles in the cross pattern (The initial, bounce-back and landing coordinates of the projectile are marked in the figure.). (a) α=0˚, (b) α=10˚, (c) α=20˚**

## S7 Experimental and theoretical comparison of four connection patterns

In what follows, the experimental results are used to validate the model for the flight of the projectiles, according to Eq.(S1) When the launching angle α=0˚, the average exit velocity of the projectiles is measured to be 3.42 m/s. The x-z coordinate data of the No. 1 projectile are taken for the flight experiment in the double-projectile connection pattern. The data of the No. 2 projectile are taken from the other three experiments, respectively. The coordinates are plotted along with their theoretically calculated counterparts in.

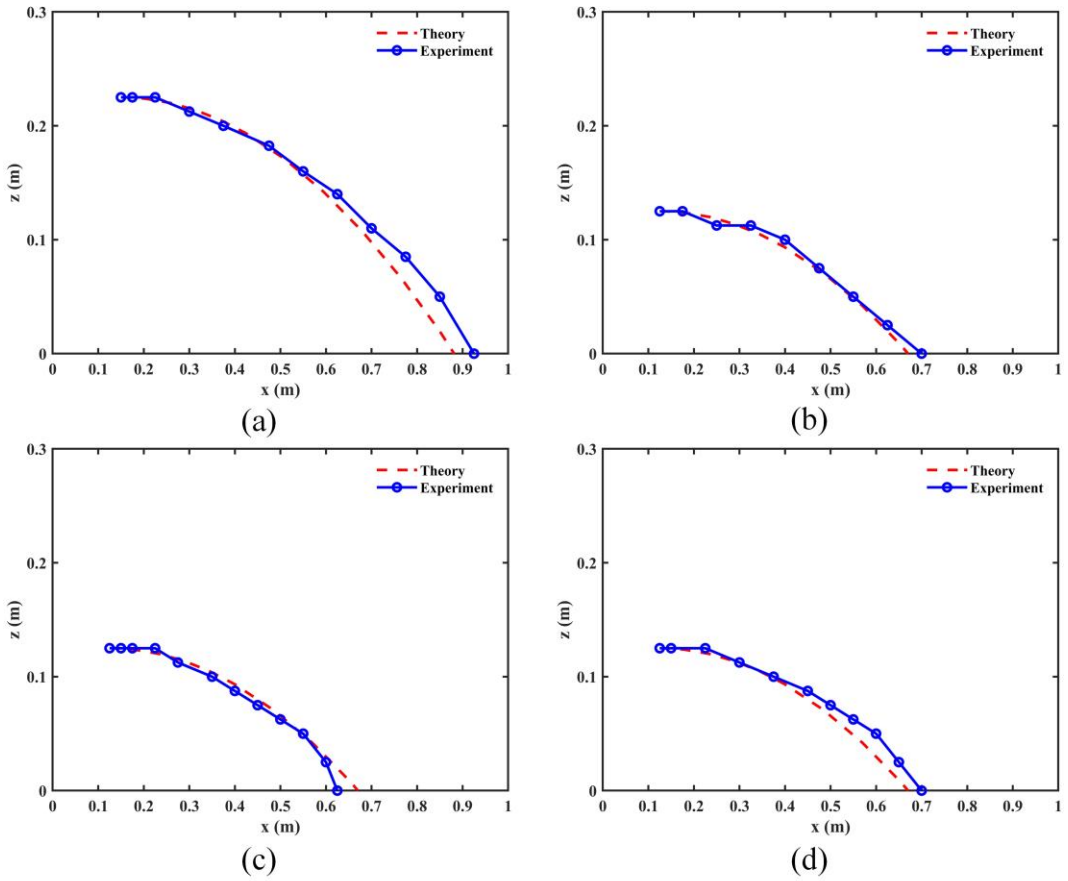


**Fig. S7 Theoretical and experimental flight coordinates of the projectiles when the launching angle α=0°. (a) the double-projectile pattern, (b) the rectangular pattern, (c) the cross pattern, (d) and the wiring pattern**

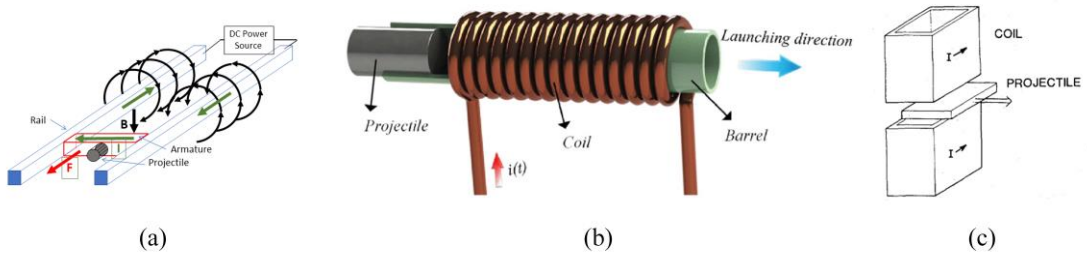


**Fig. S8 Three types of the electromagnetic launching devices.(a) rail launcher, (b)coil launcher, (c) reconnection launcher**

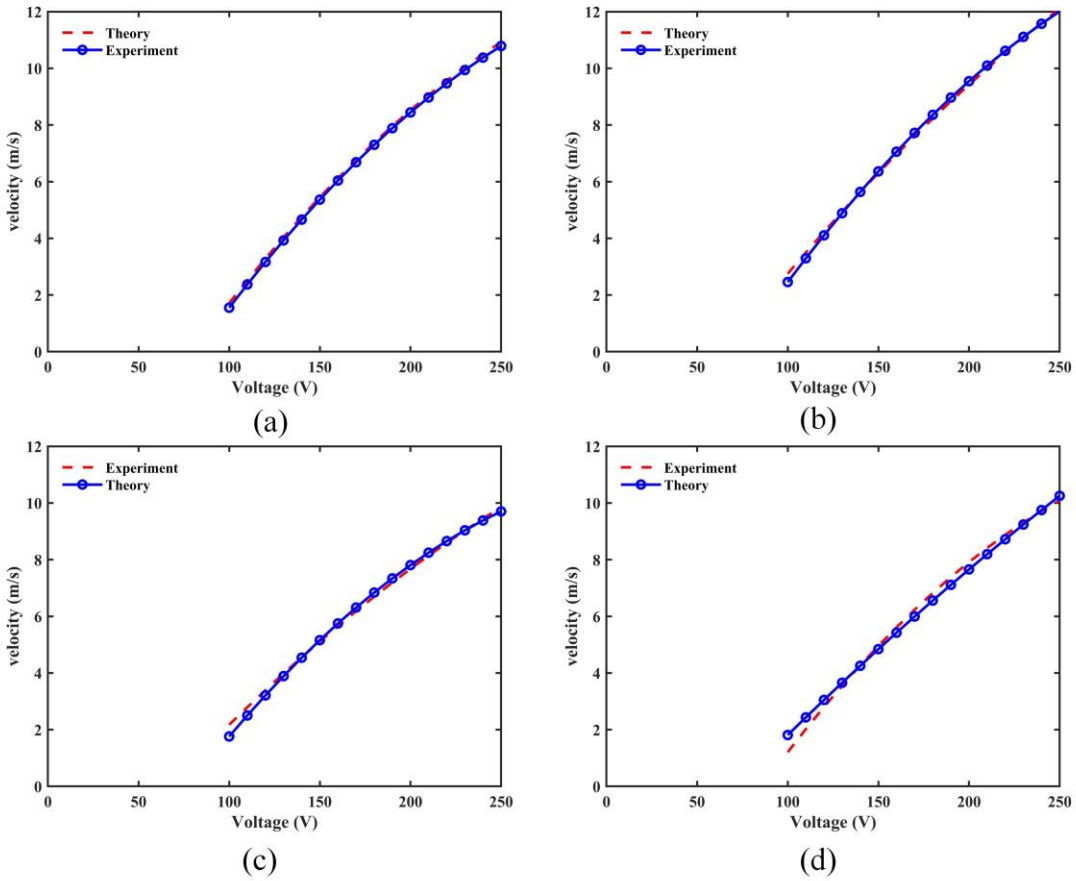


**Fig. S9 Measured exit velocities of the projectile under different charged voltage and wire diameters: (a) 0.4 mm wire; (b) 0.6 mm wire; (c) 0.8 mm wire; (d) 1 mm wire**

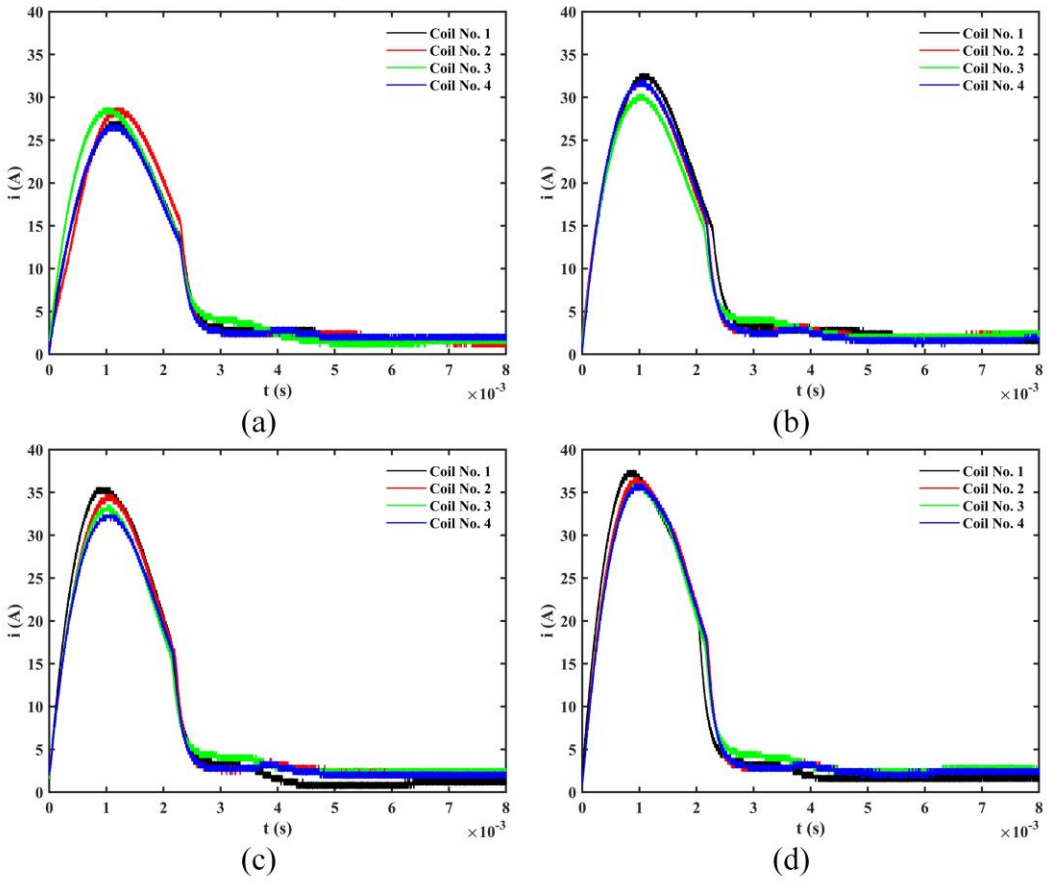


**Fig. S10 Time history of the current in the coils during launching under different charged voltage on the capacitor: (a) under 100 V charged voltage ; (b) under 110 V charged voltage; (c) under 120 V charged voltage; (d) under 130 V charged voltage**

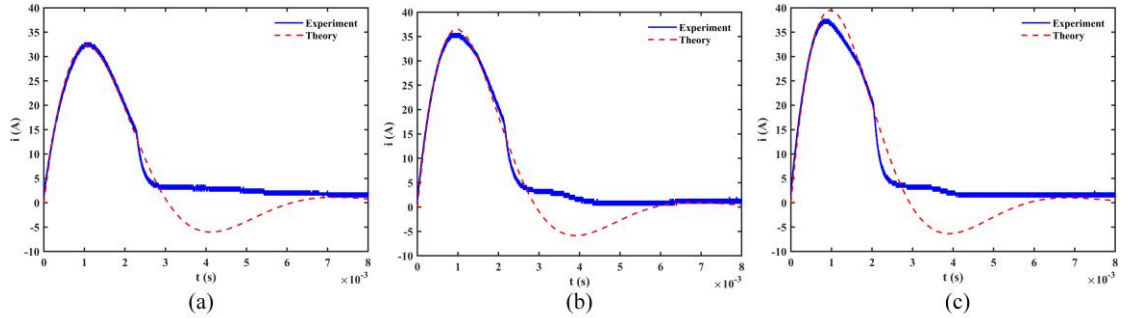


**Fig. S11 Time history of the current in the coils during launching under different charged voltage on the capacitor: (a) under 110 V charged voltage; (b) under 120 V charged voltage; (c) under 130 V charged voltage**

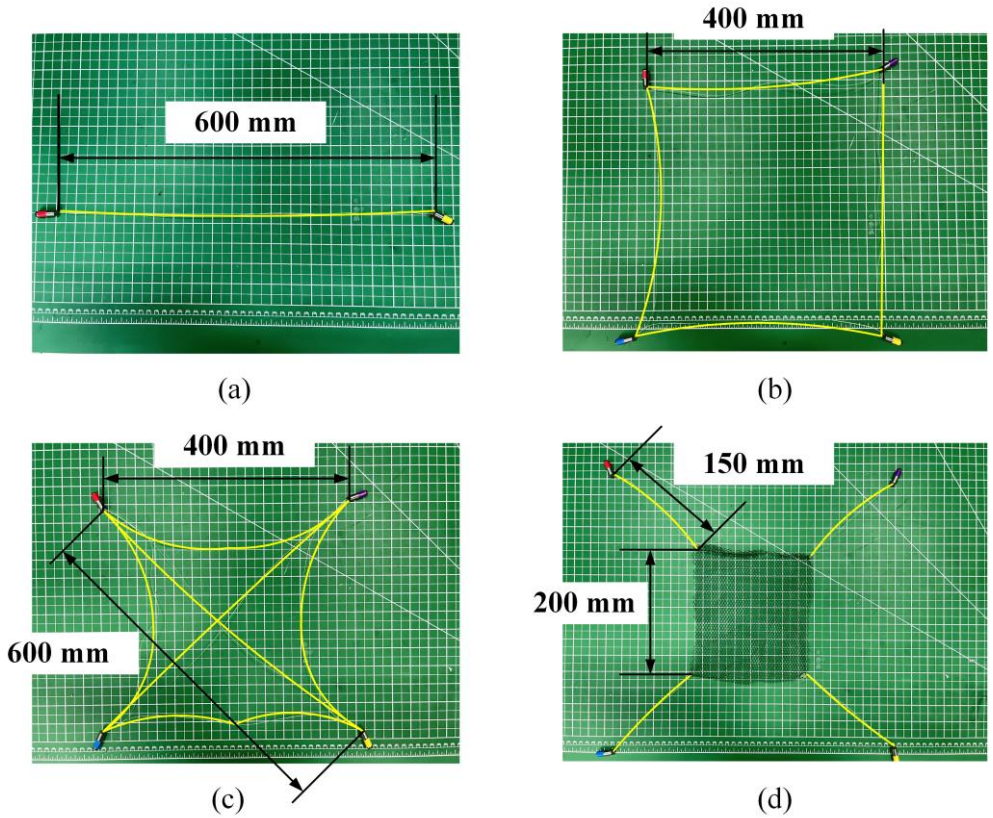


**Fig. S12 Different connection patterns between the projectiles and the approximate net(The fishing line in the figure is too thin so that marked with yellow to make it clear). (a) the double-projectile pattern, (b) the square pattern, (c) the cross pattern, (d) and the wire pattern**

**Table S1 Coil parameters of different wire diameters**

| Coil group | Wire diameter (mm) | Resistance $R_c$ $(\Omega)$ | Inductance $L_c$ (mH) | No. of turns |
|---|---|---|---|---|
| 1 | 0.4 | 3.5 | 1.55 | 600 |
| 2 | 0.6 | 1.5 | 0.95 | 420 |
| 3 | 0.8 | 0.6 | 0.70 | 320 |
| 4 | 1.0 | 0.3 | 0.22 | 170 |

**Table S2 Parameters of different numbered coils**

| Coil number | Resistance $R_c$ $(\Omega)$ | Inductance $L_c$ (mH) | No. of turns |
|---|---|---|---|
| 1 | 1.8 | 1.94 | 420 |
| 2 | 1.8 | 1.96 | 420 |
| 3 | 1.9 | 2.04 | 420 |
| 4 | 1.9 | 1.96 | 420 |